applied sciences

MDPI

Review

Molecular Dynamics of XFEL-Induced Photo-Dissociation, Revealed by Ion-Ion Coincidence Measurements

Edwin Kukk [1,*], Koji Motomura [2], Hironobu Fukuzawa [2,4], Kiyonobu Nagaya [3,4] and Kiyoshi Ueda [2,4]

1 Department of Physics and Astronomy, University of Turku, FI-20014 Turku, Finland
2 Institute of Multidisciplinary Research for Advanced Materials, Tohoku University, Sendai 980-8577, Japan; motomura@tagen.tohoku.ac.jp (K.M.); fukuzawa@tagen.tohoku.ac.jp (H.F.); ueda@tagen.tohoku.ac.jp (K.U.)
3 Department of Physics, Graduate School of Science, Kyoto University, Kyoto 606-8502, Japan; nagaya@scphys.kyoto-u.ac.jp
4 RIKEN Spring-8 Center, Sayo, Hyogo 679-5148, Japan
* Correspondence: edwin.kukk@utu.fi

Academic Editor: Malte C. Kaluza
Received: 24 March 2017; Accepted: 12 May 2017; Published: 19 May 2017

Abstract: X-ray free electron lasers (XFELs) providing ultrashort intense pulses of X-rays have proven to be excellent tools to investigate the dynamics of radiation-induced dissociation and charge redistribution in molecules and nanoparticles. Coincidence techniques, in particular multi-ion time-of-flight (TOF) coincident experiments, can provide detailed information on the photoabsorption, charge generation, and Coulomb explosion events. Here we review several such recent experiments performed at the SPring-8 Angstrom Compact free electron LAser (SACLA) facility in Japan, with iodomethane, diiodomethane, and 5-iodouracil as targets. We demonstrate how to utilize the momentum-resolving capabilities of the ion TOF spectrometers to resolve and filter the coincidence data and extract various information essential in understanding the time evolution of the processes induced by the XFEL pulses.

Keywords: free electron laser; Coulomb explosion; radiation damage; molecular dynamics; X-ray absorption; ultrafast dissociation; coincidence; photoion-photoion coincidence (PIPICO); ion mass spectroscopy; time-of-flight

1. Introduction

Nuclear motion in molecules and clusters takes place in a timescale starting from a few femtoseconds. Photoinduced nuclear dynamics—isomerization, bond breakage and dissociation, Coulomb explosion of molecules and clusters, chemical reactions—have long been of particular interest from both the fundamental and applied points of view [1–3]. In order to accurately observe such motion and trace its development, a sufficiently short initiating pulse of radiation is needed as not to obscure the real dynamics. Lasers have provided such an excitation source. The advent of free electron lasers (FELs) operating in the UV- and X-ray regime, however, opened up completely new avenues, providing access to tunable atomic inner-shell multiphoton excitation and ionization in femtosecond timescales [4–11]. In the present paper, we focus on the unimolecular dissociation reactions induced by intense femtosecond-range X-ray pulses of FEL radiation. Specifically, we present examples on how to extract detailed information about the nuclear, and also the related electron dynamics by using coincident ion spectroscopy and momentum filtering analysis methods. The full results of these experiments and their interpretation are published or submitted for publication elsewhere, in [12] for CH_3I, in [13] for CH_2I_2, and in [14,15] for 5-iodouracil.

In order to reconstruct the dissociation process, as much information as possible should be gathered from each dissociation event; ideally this means detecting all atomic and molecular fragments (of all charges), as well as emitted electrons, and measuring their momenta. In practice, it would be a formidable task for all but the simplest systems and processes. Various experimental set-ups, as well as analysis methods, have been developed towards this goal. Most usable at FEL sources so far have been electron and ion time-of-flight (TOF) spectrometers and their various developments, such as COLTRIMS for ion-electron coincidences [16,17], and magnetic bottle spectrometers for electrons [18–23].

The results presented in this article are based on experiments performed at SACLA XFEL in Japan, using momentum-resolving ion TOF spectrometers with multi-ion detection capabilities per FEL pulse [24]. The multi-ion detection offers the opportunity for performing *coincidence* (specifically ion-ion or multi-ion coincidence) analysis. In coincidence methods, each event is analyzed separately, tracing back the detected ions to a single source—an ionized and subsequently dissociating molecule, cluster, or nanoparticle. By its nature, it is one of the most accurate approaches in experimentally reconstructing the quantum mechanical event [25–29].

Coincidence experiments at FEL sources also face major challenges. Firstly, the repetition rates of FEL sources have been relatively low, even as low as 10 Hz for SACLA, which means that collecting sufficient coincidence data is a lengthy process during the extremely valuable beamtime (once referred to as a "heroic experiment" by a referee). This limitation is gradually becoming less severe with, for example, the Linac Coherent Light Source (LCLS) operating at 120 Hz and the European XFEL shortly starting operations at the planned 27,000 pulses per second. The second limitation is more fundamental, namely that for efficient coincidence analysis it must be ensured that all detected fragment ions indeed originate from the same event. Otherwise, the combinations of ions from different sources would be meaningless and create erroneous data, often referred to as "false coincidences". It can be a particularly severe problem at FEL sources, since the pulses have very high photon density (often desirable for a specific process to occur), creating many ionization events per pulse while, for a coincidence experiment, the ideal would be a single ionized particle per pulse. As a simplified example, in an (N^+, N^+) coincidence analysis of the photodissociation of N_2, only 20% are proper ("true") coincidences if three molecules are ionized by the FEL pulse; and only 2% if 25 molecules are ionized. In the latter regime (which is not uncommon in a FEL experiment), coincidence analysis would be overwhelmed by the false coincidences, without additional means of distinguishing them from the true ones.

One solution to this predicament is to perform *covariance* analysis, in which statistically significant relationships between various detected particles are looked for, not on an event-by event basis, but by using statistical analysis methods [30–34]. Covariance analysis has been shown to extract useful information even from datasets with high ionization rates per pulse. The second solution is to utilize additional information in sorting the raw data into coincidence events. Modern ion TOF spectrometers equipped with accurate position-sensitive detectors are capable of recording the data for complete ion momentum reconstruction. On the same example of N_2 above, one can confidently assume that the true coincident ions should have the momentum vectors antiparallel and of equal length, as to satisfy the momentum conservation. That condition can be used as a very efficient filter, dramatically increasing the true/false coincidence ratio and making a coincidence analysis possible at seemingly too high ionization rates. Naturally, the above example is trivial, but similar physically justified momentum filtering (hereafter referred to as MF) conditions can often also be found in significantly larger systems.

In the present paper, we present three systems of increasing complexity (Figure 1)—iodomethane (CH_3I) possessing a three-fold symmetry axis, diiodomethane (CH_2I_2) with two symmetry planes, and a planar molecule 5-iodouracil ($C_4H_3IN_2O_2$). We show how multi-ion coincidence analysis can be applied in combination with the MF as a powerful tool for extracting information on femtosecond-scale molecular dynamics.

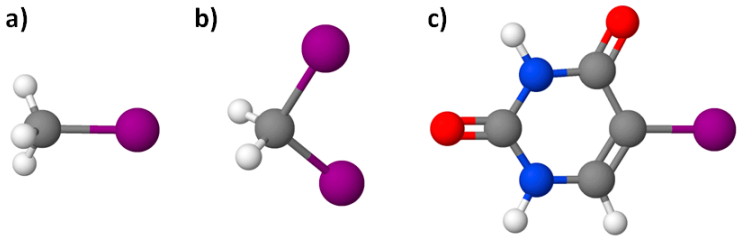

Figure 1. The molecules studied: (**a**) iodomethane, (**b**) diiodomethane, and (**c**) 5-iodouracil. Pink—iodine, blue—nitrogen, red—oxygen, gray—carbon, and light gray—hydrogen.

2. Materials and Methods

The experiments were carried out at beam line 3 (BL3) of the SACLA X-ray free electron laser (XFEL) facility [35] and are described in detail in [12–15]. The XFEL beam is focused by the Kirkpatrick-Baez (KB) mirror system to a focal size of about 1 μm (FWHM) diameter. The photon energy was set to 5.5 keV and the photon bandwidth was about 40 eV (FWHM). The repetition rate of the XFEL pulses was 10 (for CH_3I and 5-iodouracil) or 30 Hz (for CH_2I_2). The pulse duration was estimated to be about 10 fs. The peak fluence was estimated to be 26 $\mu J/\mu m^2$ in the CH_3I and 5-iodouracil experiment, and 26 $\mu J/\mu m^2$ in the CH_2I_2 experiment.

The gas phase samples were introduced to the focal point of the XFEL pulses as a pulsed supersonic gas jet seeded by helium gas. The ions were detected by a multi-coincidence recoil ion momentum spectrometer to measure three-dimensional momenta of each fragment ion (see Figure 2).

The molecular beam was crossed with the focused XFEL beam at the reaction point and the emitted ions were projected by electric fields onto a microchannel plate (MCP) detector in front of a delay-line anode (Roentdek HEX80, by RoentDek Handels GmbH, Kelkheim, Germany). We used velocity-map-imaging (VMI) electric field conditions. Signals from the delay-line anode and MCP were recorded by a digitizer and analyzed by a software discriminator. The arrival time and the arrival position of each ion were determined and allowed us to extract the three-dimensional momentum of each ion.

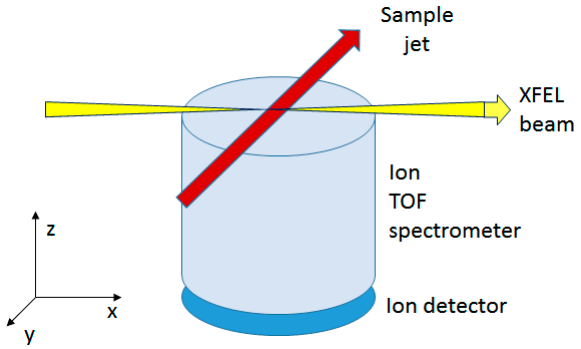

Figure 2. Sketch of the experimental setup at SPring-8 Angstrom Compact free electron LAser (SACLA).

An essential element in interpreting the observations in all three cases was a comparison with a rather simple Coulomb explosion model, predicting the fragments' momentum vector correlations, magnitudes and geometry. Such quick, empirical models proved an invaluable aid in data analysis and we, thus, summarize its main properties. The classical point charge model assumes the source of the total charge creation to be the heavy (in this case iodine) atom, due to its much higher photoionization cross-section at around 5 keV. The charge build-up is described statistically as a smooth function:

$$Q_{tot}(t) = Q_{tot,final}\left(1 - \exp\left(-\frac{t}{\tau}\right)\right), \quad (1)$$

where τ is the empirical, adjustable charge build-up constant. In comparison with the experiments, we found τ close to 10 fs in all cases. The positive charge is multiplied by additional absorption and by Auger cascades, transferring charge from iodine (Q_I) to the rest of the molecule (Q_X):

$$\frac{dQ_X(t)}{dt} = R \times Q_I(t), \tag{2}$$

where R is the charge transfer rate—another empirical constant in the model. The fragment momenta and their correlations is a sensitive function of the charge dynamics and the above-given model parameters.

3. Results and Discussion

3.1. Iodomethane

CH_3I molecules were irradiated with ultrashort ($\sim$ 10 fs) XFEL pulses of 5.5 keV energy. The experimental results, as well as the Coulomb explosion modeling, was published in [12]; here we summarize them as far as necessary for the coincidence analysis' background.

The molecules absorb X-rays predominantly in the iodine atomic site, where electrons from inner shells down to I 2p are emitted. Multiphoton absorption occurs during the pulse and the charge is also further increased by Auger cascades, as demonstrated in the case of xenon—an atom with a very similar electronic structure [36,37]. The Auger cascades are also the most likely mechanism of transferring charge to the methyl group of the molecule. The highly-charged molecule undergoes Coulomb explosion, producing the I^{n+}, C^{m+}, and $H^{0,1+}$ fragments. Ion-ion coincidence analysis of these fragments was detected by the momentum-resolving ion TOF spectrometer, which then provided the data to reconstruct the dynamics of the dissociation events.

The ion count per XFEL pulse was quite high, with the average of 7.25 heavy (excluding H^+) ions/pulse. Assuming an ion collection and detection efficiency of roughly 50% means that in average of about 7 molecules/pulse were ionized; quite unfavorable conditions for coincidence analysis. Under such conditions, the most informative approach was, mainly, to perform a two-particle ion-ion coincidence (PIPICO) analysis with the help of MF.

A possible pitfall in the MF-enhanced PIPICO lies in carrying over the filtering conditions to the result and erroneously interpreting the apparent correlations as coincidence information, while they were just created by the filtering process. To avoid this, we used several strategies. First, the MF can be performed using only two momentum vector components on the detector plane perpendicular to the TOF spectrometer's axis (See Figure 2). That leaves the third axial component undisturbed and, if a clear PIPICO pattern emerges in the first ion's TOF versus the second ion's TOF plot, it is a confirmation that true coincidence events were found. Second, the measured events can be "scrambled" by redistributing the individual ions between the events. Scrambling ensures that there are no true coincident ion pairs left in the data and, thus, all remaining apparent correlations, if any, must be assigned to the MF action and discarded.

We first present an example of the analysis of a coincident pair (I^{5+}, C^{2+}) that has the best counting statistics. At first, ion pairs are formed from all events with no filtering nor bias—if, for example, one iodine and two carbon ions are detected in a pulse, a pair is formed by randomly choosing one of the carbons. A momentum sum plot is then generated and is shown in Figure 3a, where the direction of the iodine's momentum is always pointing along the x-axis. It is seen from Figure 3a, that there is a diffuse background of uncorrelated momenta and a bright spot that corresponds to well-correlated momenta. However, the bright spot is not centered at zero; its shift indicates that the iodine's momentum is larger than the carbon's. This is easily understood from the molecular geometry: both the H^+ and C^{2+} ions balance the momentum of I^{5+}, but the H^+ momenta are not included in the sum. This "dark" momentum is manifested as the shift of the correlated spot. However, it is also seen that the spot is well defined in the y-direction, meaning that the three hydrogens carry a concerted

momentum that is directed closely along the C-I bond. In short, the momentum sharing between I and C ions can be, based on Figure 3a, approximated by a two-body dissociation if the C momentum is corrected by a dark momentum coefficient k:

$$p_{I,x} = -(p_{C,x} + 3p_{H,x}) = -\frac{1}{k}p_{C,x}.$$

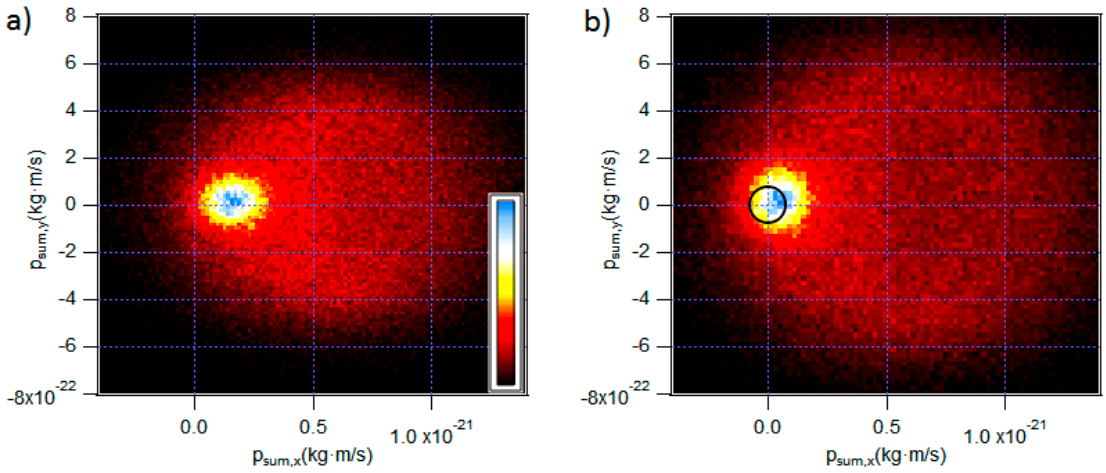

Figure 3. Momentum sum plots on the detector plane of the two ions in the (I^{5+}, C^{2+}) coincident pairs of iodomethane. The pairs were rotated to point the momentum of I^{5+} in the x-direction. (**a**) Applying the correction coefficient k = 1, (**b**) k = 0.78. The black circle illustrates the strength of the MF, applied later.

As the next step, the correct value of this coefficient is determined by applying a two-dimensional MF and restricting the momentum sum of acceptable pairs on the detector plane to a small circle around zero. The value of the coefficient k is scanned and the filtered coincident pair count obtained for each value, with the result shown in Figure 4. It shows a clear maximum at $k = 0.78 \pm 0.02$. When we now regenerate the momentum sum plot with this coefficient, but without applying the MF (Figure 3b), it has the characteristics of a two-body process: a circular diffuse false coincidence background and the true coincidence spot close to zero. Misleadingly, the spot still appears not exactly centered at zero. This is an artifact of the rotation to point $\mathbf{p}_I$ always in the x-direction, and warrants a brief discussion in Appendix A.

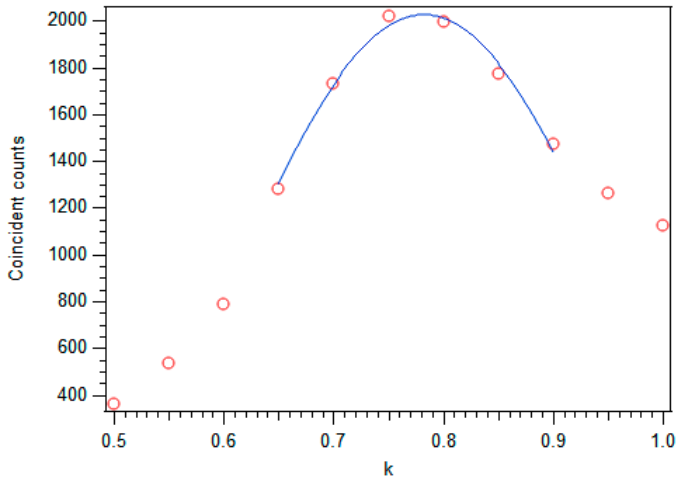

Figure 4. Coincident pair (I^{5+},C^{2+}) counts as a function of the dark momentum coefficient k.

To verify that we have obtained true coincidences, a PIPICO plot is shown in Figure 5a, obtained with the correction coefficient $k = 0.78$, but not applying MF. Here one can see both the true coincidences as a tilted rectangular pattern and the false coincidence background as the fainter rectangle. The tilted pattern is the result of correlation in the axial momentum component, not used for MF. This pattern can be improved by applying the MF to the detector plane, as shown in Figure 5b, where a much sharper PIPICO pattern with almost no background is seen. The strength of the MF is indicated in Figure 3 by the black circle, although the events were chosen from within this circle in the *unrotated* image, not in the rotated one (see Appendix A) (there was a technical problem in this experiment that resulted in an increased ion source size along the TOF axis. The strong filtering applied resulted also in ions accepted only from part of the source and created a narrower tilted pattern).

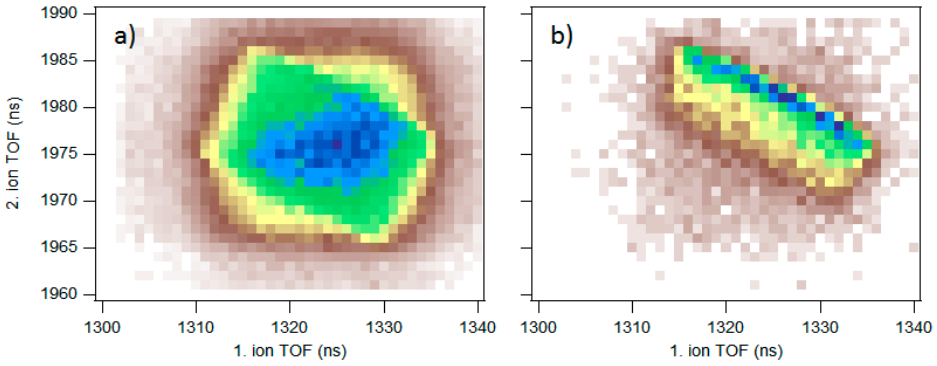

Figure 5. Photoion-photoion coincidence (PIPICO) maps of the (I^{5+}, C^{2+}) coincidences, (**a**) without momentum filtering (MF), and (**b**) with two-dimensional MF applied.

We also demonstrate an application of the MF to a difficult case where no PIPICO pattern is initially discernible at all—the (I^{11+},C^{3+}) coincidences. Here, the I^{11+} ions (with m/q of 11.5) are completely buried under the strong and broad C^+ peak in the ion TOF spectrum. The initial creation of the unfiltered and unbiased ion pairs produces a momentum sum plot in Figure 6a that is dominated by false coincidences (mostly between C^+ and C^{3+}), but a weak coincident spot of I^{11+},C^{3+} is also seen as a slight enhancement of the intensity just right of the (0,0) position in the plot.

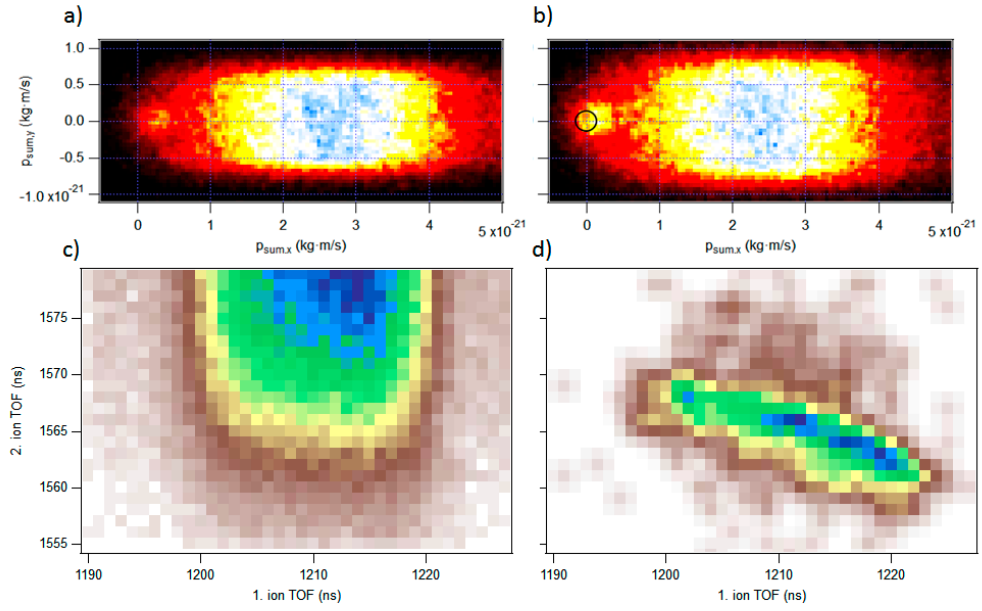

Figure 6. Momentum sum plots (**a**) and (**b**) and PIPICO plots (**c**) and (**d**) of (I^{11+}, C^{3+}) coincidences.

The PIPICO plot in Figure 6c does not show any typical tilted pattern. Repeating the procedure described before, we first obtain the correlation coefficient, $k = 0.825$, and recreate the momentum sum plot (Figure 6b). For this plot, the lowest-strength MF is applied—the momentum sum is not restricted to a certain maximum length, but a set of ion pairs was formed that gave the best momentum correlation, instead of forming pairs randomly. Finally, strong MF is applied on the detector plane (eliminating 97.8% of the ion pairs), as indicated with the black circle in Figure 6b. A PIPICO pattern now emerges clearly, as seen in Figure 6d.

Since the coincidences are extractable from the (I^{11+}, C^{3+}) pairs, let us attempt to also derive the kinetic energy distributions of the ions from this most difficult case in our dataset. The results are shown in Figure 7, where first the curves were extracted for the (I^{11+}, C^{3+}) set using MF to remove false coincidences. However, even the filtered data still contains a number of false coincidences from the diffuse background (see Figure 6b, for example). In order to remove that, the filtering was also applied to a *scrambled* dataset, where iodine ions were always paired with carbon ions from a different event (XFEL pulse) and which contained only false coincidences. The final kinetic energy distributions were obtained by subtracting the scrambled distributions. In the case of C^{3+}, for example, it is seen from Figure 7 that the false coincidences mostly contribute to the lower kinetic energies: this is since most of the C^{3+} ions come from other events with iodine charges lower than 11+ and, thus, with lower energy release.

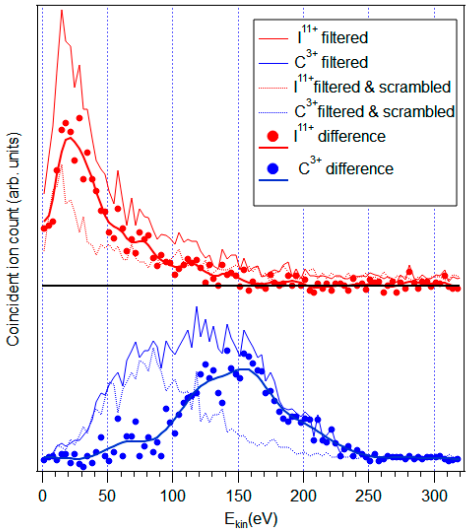

Figure 7. Kinetic energy distributions of ions in the (I^{11+}, C^{3+}) coincidences. Top panel: I^{11+}, bottom panel: C^{3+}.

Briefly, the complete analysis similar to the procedures described here allowed us to draw important conclusions on the interplay of the electron and nuclear dynamics during short XFEL pulses. We found that the C-I bond has only time to elongate only 10% or even less during the 10 fs pulse, whereas the C-H distances are nearly tripled [12]. These results are rather different from the ones predicted by instantaneous charge creation and redistribution.

3.2. Diiodomethane

In diiodomethane that contains three heavier atoms, one does not expect to find two-ion coincidences that can be well-approximated by a two-body dissociation process. However, the geometry suggests that, at least in the cases where the charge distribution between the two iodine atoms is not very unbalanced, a similar approach than for CH_3I could be useful. We, therefore, assume that the C ion is well momentum correlated with the *combined* momenta of the two I ions, but that some momentum is removed by the hydrogens along the direction of the carbon momentum. This is supported by point-charge Coulomb explosion simulations.

A test of this approach is presented on the example of a triple-coincidence set, (I^{3+}, I^{3+}, C^{2+}). In a dark momentum coefficient scan, such as in CH_3I, the triple coincident count reaches maximum at around $k = 0.75$, although in this case the maximum is not as sharply defined as in CH_3I. The triple momentum sum plot, after applying the correction coefficient to the carbon momentum, is shown in Figure 8. An alternative would be to apply the dark momentum correction to the combined momentum of the two iodine atoms, reducing it instead of increasing the carbon momentum. Both approaches gave very similar results. In Figure 8 one can see a rather well defined true coincidence region (again there is a slight displacement of it from the origin, for the same reason as discussed above).

For triple coincidences, a more informative representation than PIPICO plots is, for example, a Newton plot, as shown in Figure 9. The plot was obtained by applying MF with the strength as indicated by the circle in Figure 9, but in order to further reduce the false coincidence contributions, the filter was applied in all three dimensions (restricting the full vector sum to within a sphere around zero). The MF, itself, does not define any structures in the Newton plot, as it only restricts the three-vector sum values not, for example, the angle between the iodine ions. In generating Figure 9, all momenta of the first I^{3+} ion in the set were rescaled to 1×10^{-21} kg·m/s and rotated onto the x-axis. The red spot is the distribution of the second iodine ion's momenta and the blue spot shows the momenta of carbon ions. The black dots are the calculated momentum vectors from a point-charge Coulomb explosion simulation. For the simulation, the initial positions of the charges were fixed according to the ground state equilibrium geometry of diiodomethane, full charges were assigned instantaneously to the atoms and then their classical trajectories were followed. The comparison with the experimental momentum islands in Figure 9 shows a very good agreement in the angular distribution, but a clearly shorter vector length for the carbon ions, indicating that in the Coulomb explosion they obtain a lesser share of the kinetic energy release than predicted by the simplest model. Detailed investigations of the Coulomb explosion's dynamics in CH_2I_2 can be found in [13].

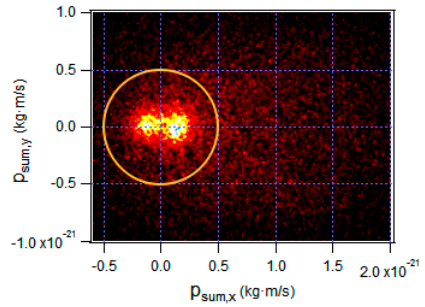

Figure 8. Momentum sum plot of (I^{3+}, I^{3+}, C^{2+}) triple coincidences. The circle illustrates the strength of the three-dimensional MF applied afterwards. The sum of the iodine momenta is directed along the x-axis.

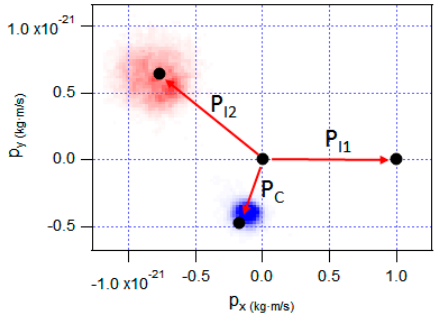

Figure 9. Newton plot of the (I^{3+},I^{3+},C^{2+}) triple coincidences, with the first I^{3+} ion's momentum in the x-direction and normalized to 1×10^{-21} kg·m/s. The red-coloured area marks the second I^{3+} ion's momenta and the blue-colored area the C^{2+} ion's momenta. Black dots are from point-charge Coulomb explosion simulation.

Finally, Figure 10 displays an ion-ion coincidence plot between the C^{2+} and I^{3+} ions in the (I^{3+},I^{3+},C^{2+}) triple coincidence set, after applying the same MF as for the Newton plot. The emission angle of about 107° between the two ions (see Figure 9) results in an elliptical PIPICO island, which is also quite well represented by a simple modeling of isotropic dissociation with the angular correlation of 107° between the two ions, and using a simple linear dependency of the ion TOF from the axial velocity component. The shape of the PIPICO island is also affected by the "dark" momentum of hydrogens and by the nonlinearity of the dependency of ion TOF from the axial velocity.

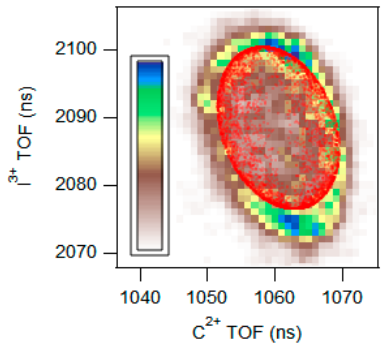

Figure 10. (C^{2+}, I^{3+}) PIPICO plot from the (I^{3+}, I^{3+}, C^{2+}) coincidence set in CH_2I_2. Color map: experiment, red dots: model.

3.3. 5-Iodouracil

The last molecule in the series studied at SACLA is 5-iodouracil, a cyclic planar molecule. Extracting high-quality coincidence datasets by MF is, on one hand, more difficult in this case because no clear axis of momentum distribution exists and it is shared by a number of ions. On the other hand, the ionization rate/pulse was relatively low in this experiment [14,15]. Here, again, preliminary Coulomb explosion simulations are valuable in deciding the strategy of applying MF. Modeling suggested, first, that the ion trajectories are significantly affected by their initial vibrational motion, which should, therefore, be added to the model. Second, the ion momenta are not expected to remain planar (due to vibrations) but strong deviations can occur. Planarity is, therefore, not the best criterion for the MF. Third, the carbon ions, being surrounded by heavier elements, have very variable trajectories that bear little resemblance to the original geometry and, therefore, are not the best candidates to be included in MF. On the other hand, oxygen ions, being on the outer positions, have trajectories that reflect well the geometry of the ring and also have sufficiently high momenta for efficient filtering. However, the lack of axial symmetry means that the filtering should be done based on the *angle* between the momenta, rather than the length of their sum. We will demonstrate this type of MF on the cases of triple coincidence sets containing the two oxygen ions. Figure 11 shows the angular correlations between the momenta of the ions in the (O^+,O^{2+},H^+) triple coincidence set and confirms the predictions of the simulations: the O^+,O^{2+} angle has a strong correlation maximum at around 115°, while the planarity of the three vectors is not sharply defined (although the dissociation is preferentially planar).

Next, we extract triple coincidence sets with angular correlation MF for the two oxygen ions. Figure 12 shows a Newton plot for the (O^+, O^+, N^+) dataset. There are two possible origins for the oxygen defining the *x*-axis; these molecular orientations are depicted next to the figure. Then there are four initial positions for the N^+ ions, two of them degenerate. Indeed, the N^+ island in the figure corresponding to the degenerate position shows approximately twice the intensity of the other two. In extracting this plot, the background was slightly improved by subtracting a Newton plot generated from a scrambled coincidence set (not showing any defined islands). The conical sharp limits of the O^{2+} island is the result of applying the angular MF.

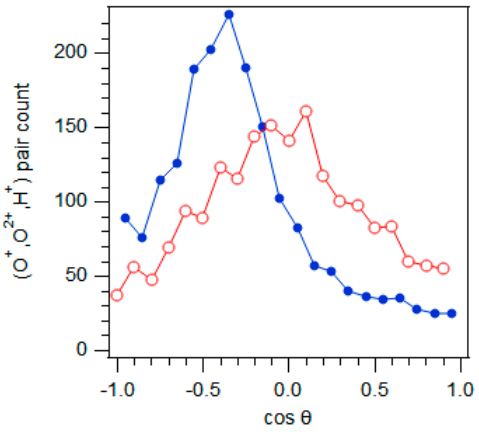

Figure 11. Distribution of angles between the momentum vectors in the (O^+,O^{2+},H^+) coincidence dataset in 5-iodouracil. Blue curve with filled circles: cos(p(O^+), p(O^{2+})); red curve with open circles: cosine of p(H^+) from the (O^+,O^{2+}) momentum plane.

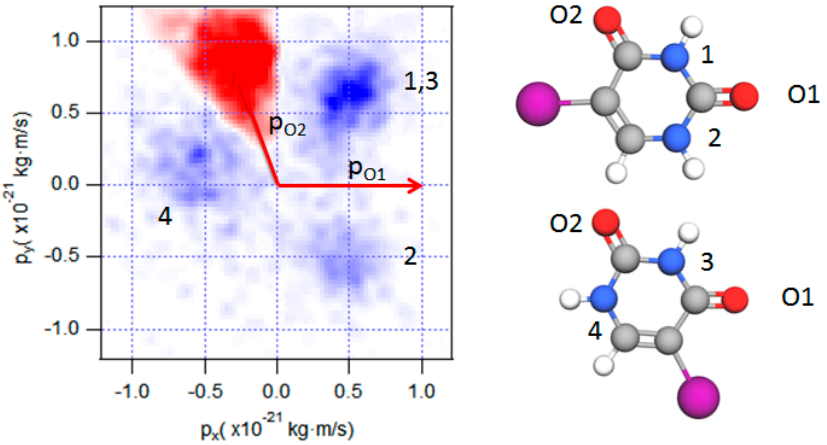

Figure 12. Newton plot of the (O^+,O^+,N^+) coincidences in 5-iodouracil, with the first O^+ ion's momentum in the x-direction and normalized to 1×10^{-21} kg·m/s, the red-colored area marking the second O^+ ion's momenta and the blue-colored area marking the N^+ ion's momenta. Possible molecular orientations and labeling of the nitrogen atoms and islands are shown to the right.

The second example is the (O^+, O^+, H^+) dataset. Due to the relatively low total charge in this experiment and the larger size of the molecule, the kinetic energies of the H^+ ions were sufficiently low for efficient detection together with the heavier ions. After applying angular MF for the two oxygens and subtracting the scrambled coincidence background, again a clear island structure emerges for the third (H^+) ion in the dataset, as shown in Figure 13. Indeed, all different initial positions of the hydrogens are discernible, indicating that the Coulomb explosion involving these ions has a common center of force in a good approximation. In contrast, we also generated Newton plots for (O^+,O^+,C^+) datasets, which showed no visible island structures for the carbon ions, in agreement with the simulations.

Interestingly, hydrogens emitted to the directions 1,4 appear to have larger momenta than the rest. Unfortunately, the number of events are not high enough to perform useful quantitative analysis of the energy distributions of ions originating from specific positions in a molecule in a particular triple coincidence dataset. Such analysis would await for FEL sources with high repetition rates. Additionally, there are indications that the probability of hydrogens from different sites acquiring charge varies somewhat, but with insufficient statistics for firm conclusions.

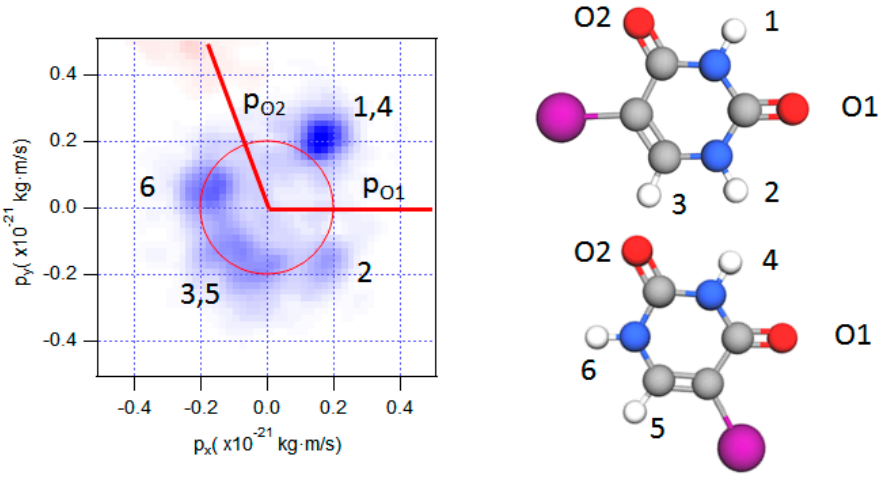

Figure 13. Newton plot of the (O^+, O^+, H^+) coincidences in 5-iodouracil. The image is slightly smoothed for better visibility. Blue-colored islands correspond to the H^+ momenta. The red circle is a guide for the eye.

4. Conclusions

We presented three cases of successful extraction and analysis of coincidence information in molecular dissociation studies with ultrashort XFEL pulses from the SACLA facility in Japan. The molecular samples possessed quite different symmetry properties, and also an increasing number of atoms from five in iodomethane to 12 in 5-iodouracil. We showed how efficient extraction of true coincidence data is achieved by applying ion momentum filtering. The exact implementation of these techniques must be flexible and adapted to the particular geometries of the samples, but is seen to work efficiently even in the case of complete atomization of a 12-atom molecule.

Coincidence techniques, proven to be powerful methods for extracting detailed information on molecular dynamics from experiments conducted at more conventional light sources, are equally valuable in FEL-based experiments. Their full potential is likely to be realized with high repetition rate sources, where the required long collection time becomes less of a restriction.

Acknowledgments: First and foremost, we are most grateful for all of the co-authors of [11,12,14,15] for their contributions in making these demanding experiments a success. The experiments were performed at SACLA with the approval of JASRI and the program review committee. They were supported by the X-ray Free Electron Laser Utilization Research Project and the X-ray Free Electron Laser Priority Strategy Program of the Ministry of Education, Culture, Sports, Science, and Technology of Japan (MEXT), by the Japan Society for the Promotion of Science (JSPS), by the Proposal Program of SACLA Experimental Instruments of RIKEN, by the IMRAM project and by the Cooperative Research Program of "Network Joint Research Center for Materials and Devices: Dynamic Alliance for Open Innovation Bridging Human, Environment and Materials". E.K. acknowledges financial support by the Academy of Finland.

Author Contributions: E.K. participated in the experiments, performed the analysis reported here and wrote the manuscript, K.M. prepared and participated in the experiments and analyzed data, H.F. planned, prepared and participated in the experiments and contributed to the analysis, K.N. prepared and participated in the experiments and analyzed the 5-iodouracil data, K.U. supervised the experimental program, participated in experiments and in the preparation of the manuscript.

Conflicts of Interest: The authors declare no conflict of interest.

Appendix A. Two-Dimensional Ion Momentum Sum Plots

Let us first assume a perfect measurement of a two-body dissociation, with $\mathbf{p}_C = -\mathbf{p}_I$. Then, before, as well as after, the rotation, $\mathbf{p}_{sum}$ is exactly zero. However, the imperfect measurement adds an uncertainty $\Delta\mathbf{p}_I$ and $\Delta\mathbf{p}_C$ to both vectors. We can make a *gedankenexperiment* where we first choose the x-axis according to the accurate vector $\mathbf{p}_I$ and then add the uncertainty $\Delta\mathbf{p}_I$. (see Figure A1). For the sake of simplicity we do not add the uncertainty $\Delta\mathbf{p}_C$. This uncertainly is directly transferred to $\mathbf{p}_{sum}$:

$\mathbf{p}_{sum} = \Delta\mathbf{p}_I$. and moves in a circle of radius Δp_I around the origin. In order to bring the vector $\mathbf{p}_I$ back on the *x*-axis, a rotation by an angle α relative to the *x*-axis needs to be performed, and with a reasonable assumption that $\Delta p_I < p_I$, $|\alpha| < 90°$. The vector $\mathbf{p}_C$ and the sum vector $\mathbf{p}_{sum}$ are naturally rotated by α as well and, thus, $\mathbf{p}_{sum}$ *always shifts in the direction of the x-axis* in rotation as a consequence of random uncertainty in the vector defining the *x*-axis. Thus, although the rotated sum momentum plots give a good visualization of the correlations and quality in the coincident dataset, they should not be used to find the correction coefficient by shifting the center of the true coincidence spot to zero—therefore, the scans, such as in Figure 4, for example, always operated on the *unrotated* momenta.

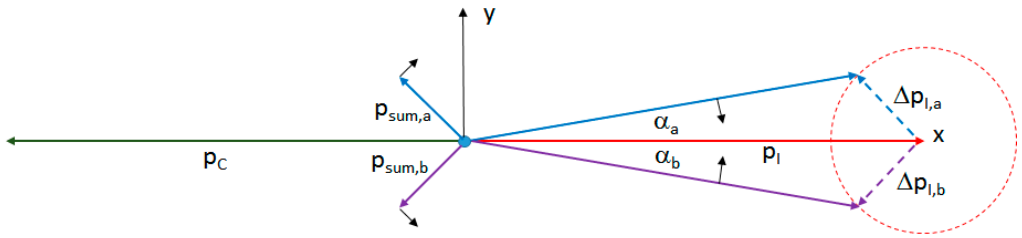

Figure A1. Sketch of the effect of the measurement error of $\mathbf{p}_I$ on the $\mathbf{P}_{sum}$ plot, with two choices a, b of the measurement error vector.

References

1. Prince, K.C.; Bolognesi, P.; Feyer, V.; Plekan, O.; Avaldi, L. Study of complex molecules of biological interest with synchrotron radiation. *J. Electron Spectrosc. Relat. Phenom.* **2015**. [CrossRef]
2. Piancastelli, M.N.; Simon, M.; Ueda, K. Present trends and future perspectives for atomic and molecular physics at the new X-ray light sources. *J. Electron Spectrosc. Relat. Phenom.* **2010**, *181*, 98–110. [CrossRef]
3. Continetti, R.E. COINCIDENCE SPECTROSCOPY. *Annu. Rev. Phys. Chem.* **2001**, *52*, 165–192. [CrossRef] [PubMed]
4. Ullrich, J.; Rudenko, A.; Moshammer, R. Free-electron lasers: New avenues in molecular physics and photochemistry. *Annu. Rev. Phys. Chem.* **2012**, *63*, 635–660. [CrossRef] [PubMed]
5. Liekhus-Schmaltz, C.E.; Tenney, I.; Osipov, T.; Sanchez-Gonzalez, A.; Berrah, N.; Boll, R.; Bomme, C.; Bostedt, C.; Bozek, J.D.; Carron, S.; et al. Ultrafast isomerization initiated by X-ray core ionization. *Nat. Commun.* **2015**, *6*, 8199. [CrossRef] [PubMed]
6. Milne, C.J.; Penfold, T.J.; Chergui, M. Recent experimental and theoretical developments in time-resolved X-ray spectroscopies. *Coord. Chem. Rev.* **2014**, *277–278*, 44–68. [CrossRef]
7. Berrah, N. Molecular dynamics induced by short and intense X-ray pulses from the LCLS. *Phys. Scr.* **2016**, *T169*, 14001. [CrossRef]
8. Bucksbaum, P.H.; Coffee, R.; Berrah, N. The first atomic and molecular experiments at the linac coherent light source X-ray free electron laser. *Adv. At. Mol. Opt. Phys.* **2011**, *60*, 239–289.
9. McFarland, B.K.; Farrell, J.P.; Miyabe, S.; Tarantelli, F.; Aguilar, A.; Berrah, N.; Bostedt, C.; Bozek, J.D.; Bucksbaum, P.H.; Castagna, J.C.; et al. Ultrafast X-ray auger probing of photoexcited molecular dynamics. *Nat. Commun.* **2014**, *5*. [CrossRef] [PubMed]
10. Minitti, M.P.; Budarz, J.M.; Kirrander, A.; Robinson, J.S.; Ratner, D.; Lane, T.J.; Zhu, D.; Glownia, J.M.; Kozina, M.; Lemke, H.T.; et al. Imaging molecular motion: Femtosecond X-ray scattering of an electrocyclic chemical reaction. *Phys. Rev. Lett.* **2015**, *114*. [CrossRef] [PubMed]
11. Tenboer, J.; Basu, S.; Zatsepin, N.; Pande, K.; Milathianaki, D.; Frank, M.; Hunter, M.; Boutet, S.; Williams, G.J.; Koglin, J.E.; et al. Time-resolved serial crystallography captures high-resolution intermediates of photoactive yellow protein. *Science* **2014**, *346*, 1242–1246. [CrossRef] [PubMed]
12. Motomura, K.; Kukk, E.; Fukuzawa, H.; Wada, S.-I.; Nagaya, K.; Ohmura, S.; Mondal, S.; Tachibana, T.; Ito, Y.; Koga, R.; et al. Charge and nuclear dynamics induced by deep inner-shell multiphoton ionization of CH3I molecules by intense X-ray free-electron laser pulses. *J. Phys. Chem. Lett.* **2015**, *6*, 2944–2949. [CrossRef] [PubMed]

13. Takanashi, T.; Nakamura, K.; Kukk, E.; Motomura, K.; Fukuzawa, H.; Nagaya, K.; Wada, S.I.; Kumagai, Y.; Iablonskyi, D.; Ito, Y.; et al. Ultrafast coulomb explosion of the diiodomethane molecule induced by an X-ray free-electron laser pulse. *Phys. Chem. Chem. Phys.* **2017**, submitted. [CrossRef]
14. Nagaya, K.; Motomura, K.; Kukk, E.; Fukuzawa, H.; Wada, S.; Tachibana, T.; Ito, Y.; Mondal, S.; Sakai, T.; Matsunami, K.; et al. Ultrafast dynamics of a nucleobase analogue illuminated by a short intense X-ray free electron laser pulse. *Phys. Rev. X* **2016**, *6*. [CrossRef]
15. Nagaya, K.; Motomura, K.; Kukk, E.; Takahashi, Y.; Yamazaki, K.; Ohmura, S.; Fukuzawa, H.; Wada, S.; Mondal, S.; Tachibana, T.; et al. Femtosecond charge and molecular dynamics of I-containing organic molecules induced by intense X-ray free-electron laser pulses. *Faraday Discuss.* **2016**, *194*, 537–562. [CrossRef] [PubMed]
16. Dörner, R.; Mergel, V.; Jagutzki, O.; Spielberger, L.; Ullrich, J.; Moshammer, R.; Schmidt-Böcking, H. Cold Target Recoil Ion Momentum Spectroscopy: A "momentum microscope" to view atomic collision dynamics. *Phys. Rep.* **2000**, *330*, 95–192. [CrossRef]
17. Ullrich, J.; Moshammer, R.; Dorn, A.; Dörner, R.; Schmidt, L.P.H.; Schmidt-Böcking, H. Recoil-ion and electron momentum spectroscopy: Reaction-microscopes. *Rep. Prog. Phys.* **2003**, *66*, 1463–1545. [CrossRef]
18. Tsuboi, T.; Xu, E.Y.; Bae, Y.K.; Gillen, K.T. Magnetic bottle electron spectrometer using permanent magnets. *Rev. Sci. Instrum.* **1988**, *59*, 1357–1362. [CrossRef]
19. Rijs, A.M.; Backus, E.H.G.; de Lange, C.A.; Westwood, N.P.C.; Janssen, M.H.M. "Magnetic bottle" spectrometer as a versatile tool for laser photoelectron spectroscopy. *J. Electron Spectrosc. Relat. Phenom.* **2000**, *112*, 151–162. [CrossRef]
20. Mucke, M.; Förstel, M.; Lischke, T.; Arion, T.; Bradshaw, A.M.; Hergenhahn, U. Performance of a short "magnetic bottle" electron spectrometer. *Rev. Sci. Instrum.* **2012**, *83*, 63106. [CrossRef] [PubMed]
21. Penent, F.; Palaudoux, J.; Lablanquie, P.; Andric, L.; Feifel, R.; Eland, J.H.D. Multielectron spectroscopy: The xenon 4D hole double auger decay. *Phys. Rev. Lett.* **2005**, *95*. [CrossRef] [PubMed]
22. Murphy, B.F.; Osipov, T.; Jurek, Z.; Fang, L.; Son, S.-K.; Mucke, M.; Eland, J.H.D.; Zhaunerchyk, V.; Feifel, R.; Avaldi, L.; et al. Femtosecond X-ray-induced explosion of C60 at extreme intensity. *Nat. Commun.* **2014**, *5*. [CrossRef] [PubMed]
23. Frasinski, L.J.; Zhaunerchyk, V.; Mucke, M.; Squibb, R.J.; Siano, M.; Eland, J.H.D.; Linusson, P.; Vd Meulen, P.; Salén, P.; Thomas, R.D.; et al. Dynamics of hollow atom formation in intense X-ray pulses probed by partial covariance mapping. *Phys. Rev. Lett.* **2013**, *111*. [CrossRef] [PubMed]
24. Motomura, K.; Foucar, L.; Czasch, A.; Saito, N.; Jagutzki, O.; Schmidt-Böcking, H.; Dörner, R.; Liu, X.-J.; Fukuzawa, H.; Prümper, G.; et al. Multi-coincidence ion detection system for EUV–FEL fragmentation experiments at SPring-8. *Nucl. Instrum. Methods Phys. Res. Sect. A* **2009**, *606*, 770–773. [CrossRef]
25. Arion, T.; Hergenhahn, U. Coincidence spectroscopy: Past, present and perspectives. *J. Electron Spectrosc. Relat. Phenom.* **2015**, *200*, 222–231. [CrossRef]
26. Eland, J.H.D.; Wort, F.S.; Lablanquie, P.; Nenner, I. Mass spectrometric and coincidence studies of double photoionization of small molecules. *Z. Phys. D Atoms Mol. Clust.* **1986**, *4*, 31–42. [CrossRef]
27. Eland, J.H.D.; Linusson, P.; Mucke, M.; Feifel, R. Homonuclear site-specific photochemistry by an ion–electron multi-coincidence spectroscopy technique. *Chem. Phys. Lett.* **2012**, *548*, 90–94. [CrossRef]
28. Rolles, D.; Pešić, Z.D.; Perri, M.; Bilodeau, R.C.; Ackerman, G.D.; Rude, B.S.; Kilcoyne, A.L.D.; Bozek, J.D.; Berrah, N. A velocity map imaging spectrometer for electron–ion and ion–ion coincidence experiments with synchrotron radiation. *Nucl. Instrum. Methods Phys. Res. Sect. B* **2007**, *261*, 170–174. [CrossRef]
29. Miron, C.; Morin, P. High-resolution inner-shell coincidence spectroscopy. *Nucl. Instrum. Methods Phys. Res. Sect. A* **2009**, *601*, 66–77. [CrossRef]
30. Card, D.A.; Folmer, D.E.; Sato, S.; Buzza, S.A.; Castleman, A.W. Covariance mapping of ammonia clusters: Evidence of the connectiveness of clusters with coulombic explosion. *J. Phys. Chem. A* **1997**, *101*, 3417–3423. [CrossRef]
31. Frasinski, L.J.; Codling, K.; Hatherly, P.A. Covariance mapping: A correlation method applied to multiphoton multiple ionization. *Science* **1989**, *246*, 1029–1031. [CrossRef] [PubMed]
32. Kornilov, O; Eckstein, M.; Rosenblatt, M.; Schulz, C.P.; Motomura, K.; Rouzée, A.; Klei, J.; Foucar, L.; Siano, M.; Lübcke, A.; et al. Coulomb explosion of diatomic molecules in intense XUV fields mapped by partial covariance. *J. Phys. B* **2013**, *46*, 164028. [CrossRef]

33. Zhaunerchyk, V.; Frasinski, L.J.; Eland, J.H.D.; Feifel, R. Theory and simulations of covariance mapping in multiple dimensions for data analysis in high-event-rate experiments. *Phys. Rev. A* **2014**, *89*. [CrossRef]
34. Mucke, M.; Zhaunerchyk, V.; Frasinski, L.J.; Squibb, R.J.; Siano, M.; Eland, J.H.D.; Linusson, P.; Salén, P.; Vd Meulen, P.; Thomas, R.D.; et al. Covariance mapping of two-photon double core hole states in C2H2 and C2H6 produced by an X-ray free electron laser. *New J. Phys.* **2015**, *17*, 73002. [CrossRef]
35. Yabashi, M.; Tanaka, H.; Ishikawa, T. Overview of the SACLA Facility. *J. Synchrotron Radiat.* **2015**, *22*, 477–484. [CrossRef] [PubMed]
36. Fukuzawa, H.; Motomura, K.; Son, S.-K.; Mondal, S.; Tachibana, T.; Ito, Y.; Kimura, M.; Nagaya, K.; Sakai, T.; Matsunami, K.; et al. Sequential multiphoton multiple ionization of Ar and Xe by X-ray free electron laser pulses at SACLA. *J. Phys.* **2014**, *488*, 32034. [CrossRef]
37. Motomura, K.; Fukuzawa, H.; Son, S.-K.; Mondal, S.; Tachibana, T.; Ito, Y.; Kimura, M.; Nagaya, K.; Sakai, T.; Matsunami, K.; et al. Sequential multiphoton multiple ionization of atomic argon and xenon irradiated by X-ray free-electron laser pulses from SACLA. *J. Phys. B* **2013**, *46*, 164024. [CrossRef]